Two-Component Vortex Flow Studies of the Colloid Core Nuclear Rocket

LOREN A. ANDERSON,* SIEGFRIED H. HASINGER,† AND B. N. TURMAN‡
Aerospace Research Laboratories (AFSC), Wright-Patterson Air Force Base, Ohio

Experiments with highly loaded solid-gas vortex flows are described. By application of end wall gas injection, solid to gas mass density ratios of the order of 100:1 have been obtained in the vortex with very small particle loss rates. Particle density distributions within the vortex were measured by x-ray absorption. Experimental data suggest a rotating fluidized bed model for the particle containment process. This concept is used to extrapolate present results to the aeromechanical design of a colloid core reactor suitable as a nuclear rocket engine.

Nomenclature

c_f = coefficient of friction
D = particle diameter
h = axial length of chamber
h_c = heat-transfer coefficient for fluidized bed
M = total powder mass in vortex
$\dot{m}$ = total gas flow rate into chamber
$\dot{m}_{ew}$ = gas flow rate into end wall injection system
R = outer radius of vortex
r = radius
T = temperature
t = time
α = $c_f\Gamma_o\rho_R/R^2\bar{\rho}$
β = $c_f\Gamma_o/Rh$
Γ_o = circulation of injected gas at periphery
Γ_r = vortex circulation at r
ε = void fraction
λ = particle loss rate coefficient
μ = gas viscosity
ρ = powder density
$\bar{\rho}$ = average powder density in fluidized bed
ρ_g = gas density
ρ_p = material density of particle
ω = angular velocity

Introduction

THE controlled nuclear fission process is an attractive potential source of energy for rocket propulsion. Currently the solid core nuclear rocket engine, exemplified by the NERVA engine, demonstrates a significant advance in performance over the chemical rocket engine. However, in the solid core reactor, nuclear fuel is imbedded in a solid structure from which the heat of reaction must be transferred to the propellant. To maintain structural integrity of the core, the core temperature as well as the core heat-transfer area are restricted, resulting in propellant temperatures which do not allow attainment of the full performance potential of the nuclear rocket. The cavity reactor, using an external moderator, attempts to relieve the structural requirements within the core by dispersing the fuel in the reactor cavity in the form of a cloud of either solid or liquid particles or, ultimately, as a gaseous cloud.[1-3] Fuel containment is provided by appropriate aerodynamic or inertial forces, or, as in the case of the nuclear light bulb concept, by a nonstructural, transparent wall. An added advantage of the cavity reactor is the relative ease of keeping the nuclear mass within criticality limits by the addition of small quantities of fuel as required.

Our present investigations are concerned with a cavity reactor which employs an inertial containment system as proposed in Ref. 3, and is referred to as the "colloid core nuclear reactor." In this system, the fuel is directly dispersed as fine particles in the propellant gas, providing intimate contact with the propellant gas and affording excellent heat-transfer conditions. Vortex flow of the propellant gas provides sufficient centrifugal force to effectively contain the particulate fuel within the reactor. This paper discusses experimental studies of particle-loaded gaseous vortex flow, and results are extrapolated to give an estimate of some operating characteristics of the colloid core reactor.

Experimental Investigations

Description of Apparatus

The vortex chamber used in the experiments is shown in Fig. 1. It was made principally of Plexiglas to allow optical and x-ray observations of the flow. Air was injected tangentially at the periphery through 12 slits of 0.03 cm width, formed by 12 overlapping vanes extending the length of the chamber. The diameter of the chamber was 30.5 cm, with length at the periphery of 6.3 cm, giving a length to diameter ratio of 0.2. On the exhaust side, the chamber had a tapered

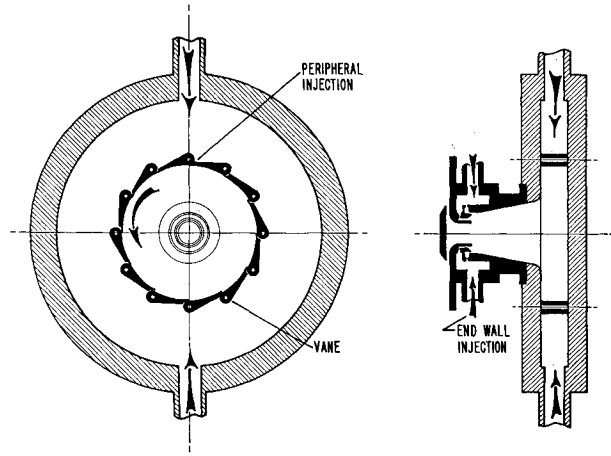

Fig. 1 End view and side view of vortex chamber.

Presented as Paper 71-637 at the AIAA/SAE 7th Propulsion Joint Specialist Conference, Salt Lake City, Utah, June 14–18, 1971; submitted July 12, 1971; revision received December 6, 1971.
Index categories: Nuclear Propulsion; Multiphase Flows.

* Former Director, Energy Conversion Research Laboratory; presently Director, Energy Conversion Research Laboratory. Member AIAA.
† Research Scientist, Energy Conversion Research Laboratory.
‡ Research Physicist, Energy Conversion Research Laboratory; Lt., U.S. Air Force.

annex with an initial diameter of 15 cm. This section was added to provide additional residence time for the separation of particles in the vortex core region. At the end of the annex was the centrally located gas outlet of the chamber. Concentric with the outlet were additional nozzles for air injection to suppress the boundary-layer flow which forms readily in confined vortices[4,5] and in the present case would transport particles to the outlet. Typical injection pressure at the periphery as well as at the end wall in the annex was around 2 atm absolute. The injection at both locations could be controlled independently and changed over wide ranges in order to study, in general, the effect of the injection split between periphery and end wall. All connections to the chamber were made flexible and the chamber itself was suspended on a beam balance to weigh directly particle addition to the vortex flow in the chamber. Sensitivity of the balance system, which used a strain gauge to detect small load changes, was about 1 gm.

Particle Properties

Particle size distributions for the three powders used in the experiments are shown in Fig. 2. The three particle species covered similar particle diameter ranges; arithmetic mean diameter was 20 μ for talc, 12 μ for tungsten, and 10 μ for zinc. Under the microscope, zinc and tungsten particles appeared almost perfectly spherical, but talc samples showed marked irregularities. These shape variations, however, should be of minor concern, since particle size was determined by a settling technique,[6] giving equivalent spherical diameters. Particle density of the different species covered a wide range, with talc density of 2.7 gm/cm^3, zinc density of 7.0 gm/cm^3, and tungsten density of 19.1 gm/cm^3. Because of the ease of operation with talc, as well as an abundant supply of the material, the bulk of these experiments were performed with talc particles, and only a limited number of runs were made with zinc and tungsten. In the following discussion, it is to be assumed that talc particles were used, unless specific mention is made of the particle species.

Powder Loading and Containment Within the Vortex

Under normal operating procedures, vortex flow in the chamber was initiated with clean air. Then a separate vortex device was used to fluidize powder and pump it into the chamber through a hole in the end wall near the periphery. The first few grams of powder added to the flow spread over most of the chamber, leaving only a clear, central region of about 5 cm diam. This amount of powder was sufficient to cause a significant decrease in the vortex rotational speed, as evidenced both from the noise level of the vortex and actual angular velocity measurements. With a total powder load

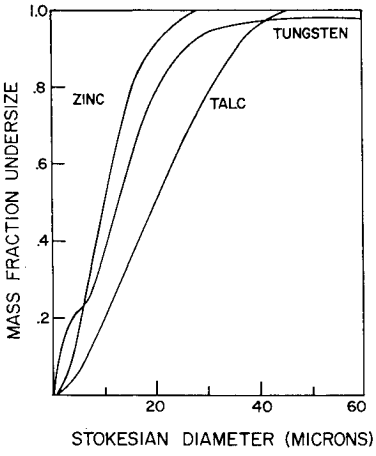

Fig. 2 Particle size distributions for powders.

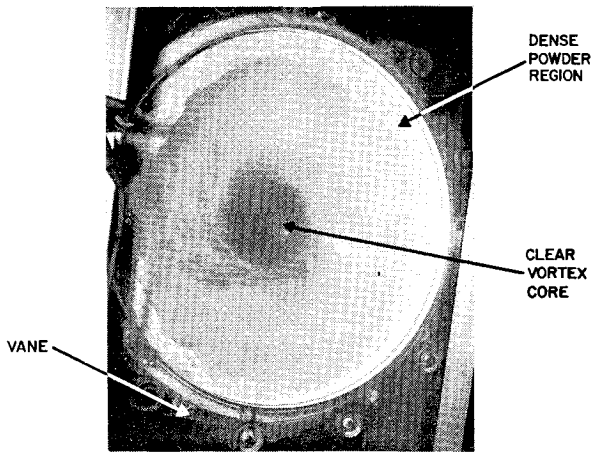

Fig. 3 Photograph of two component vortex flow.

somewhere around 50–100 gm, a dense powder bed became visible at the outer radius of the chamber, and the bed thickness increased as powder was added to the flow. The photograph in Fig. 3 illustrates the appearance of the powder flow with 400 gm powder; the clear central region is faintly discernable, along with a concentric region of low powder concentration, and a high-density powder ring on the periphery. The limit of loading was reached when the inner border of the rotating cloud extended to a diameter about equal to that of the chamber annex. The vortex then began an erratic precession, with subsequent loss of powder (as much as 10% of the maximum load).

Figure 4 summarizes observations of the functional relationship between maximum load and gas flow rate into the vortex.¶ Over the range covered by these data, there is little dependence of M_{max} on end wall fraction $\dot{m}_{ew}/\dot{m}$. To check the influence of particle properties on the maximum loading attained in the chamber, one run with zinc powder and another with tungsten powder were made, as shown in Fig. 4. Although particle mean diameters of these three particle types varied by as much as a factor of 2, with particle density varying through a factor of 7, the general trend of the talc is followed with other particle species. As a reference value, the maximum load attained here represents a particle volume fraction greater than 10%, with solid to gas mass density ratio in excess of 100:1.

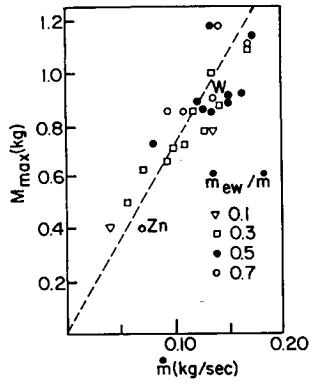

Fig. 4 Maximum powder load vs total gas flow rate, for various end wall fractions $\dot{m}_{ew}/\dot{m}$. Zinc and tungsten powder data are indicated by Zn and W, respectively.

¶ Recent experiments[7] with vortex chambers having increased axial lengths have indicated that maximum load increases somewhat less than linearly with total flow rate at higher flow rate levels.

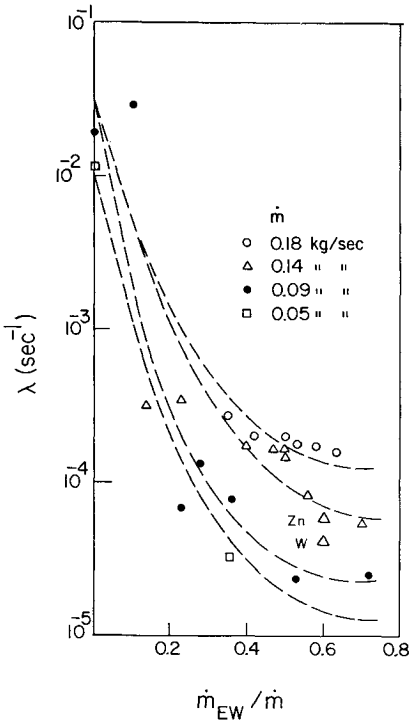

Fig. 5 Particle loss rate coefficient vs end wall fraction $\dot{m}_{ew}/\dot{m}$ for various total gas flow rates. Zinc and tungsten powder data are indicated by Zn and W, respectively.

The beam balance equipment was also used to monitor powder loss rate from the chamber. In a typical run, the chamber was loaded to a powder weight near maximum, and then powder load was recorded for a period of one hour or longer. The powder load was found to follow an exponential trend, so that a loss rate coefficient λ could be defined by

$$M = M_0 e^{-\lambda t} \tag{1}$$

where M_0 is an initial mass. An investigation of the effect of gas flow rates upon loss coefficient is summarized in Fig. 5. The importance of end wall flow is dramatically presented in this graph, which indicates a steeply rising loss rate with diminishing end wall fraction below $\dot{m}_{ew}/\dot{m} = 0.2$. These results confirm earlier indications[5] that end wall flow is essential for particle containment in a vortex. The primary need for end wall flow is in reducing or eliminating boundary flow along the chamber wall, which, if uncorrected, would entrain particles into the flow and quickly exhaust the particle load. The dependence of loss rate on total mass flow is less severe than that on end wall fraction. Since angular velocity increases with increasing $\dot{m}$, centrifugal force acting on the particle also increases, and would reduce loss rate, but a larger radial inflow velocity and turbulence level evidently yield a net increase in particle loss rate with increasing gas flow rate. Tungsten and zinc particle loss rates were somewhat lower than that for talc, as shown on Fig. 5. This trend is intuitively reasonable, because of the larger centrifugal separation effect on the denser particles.

Diagnosis of the Particle Cloud

Of particular importance for the analysis of the containment process was information regarding particle density within the vortex flow. X-ray absorption techniques have proven valuable in the area of stationary fluidized bed research,[8] and talc powder densities encountered in our rotating cloud experiment proved to be in an ideal range to utilize this method. One of the major advantages was that this technique was a completely external process, with no problem of probe disturbance. Only two-dimensional density variations could be studied, however, since the x-ray attenuation gave a particle density value which was averaged along the axial direction. The x-ray source for this experiment was a 100 kv, 15 ma medical x-ray unit: photographic film recorded x-ray intensity transmitted through the rotating particle cloud, with a typical exposure time of 1 sec. Optical density of the developed film was obtained by a photometer system, and particle mass density was subsequently deduced from these measurements.

Radial density profiles, as determined from x-ray absorption, are shown in Fig. 6. Evidence of the high-density annular cloud near the periphery is apparent here. As total powder load increases, powder bed width expands, while the average density within the bed increases to a maximum value of about 0.25 gm/cm³. This value may be compared with the loosely packed bed density of about 0.5 gm/cm³ for talc (the density obtained by simply pouring powder into a container with no agitation). A two-dimensional view of powder density for 400 gm total load is presented in Fig. 7: radial scans in Fig. 6 were made approximately through the center of the area shown in Fig. 7. The nonuniform density contours are apparently produced by the mixing process between clean air injected through the slits and the bulk of the rotating powder/air mixture. The large density islands which are located above the injected slits in Fig. 7 can be virtually eliminated by increasing the percentage of air injected through the peripheral slits. Figure 8 shows the density contours associated with the same powder load and total gas flow as that of Fig. 7, but now end wall fraction $\dot{m}_{ew}/\dot{m}$ has been reduced from 0.6 to 0.4. The increased stream energy allows the injected gas at the vanes to mix more quickly with the adjacent flow, producing a more nearly uniform fluidized flow.

To supplement average particle density measurements based on x-ray absorption, a light fiber probe was used to check the local homogeneity of the cloud. This light probe utilized two sets of light conducting fibers: one set illuminated a localized area of the particle cloud, while the second set transmitted light scattered by the particles to a photomultiplier tube outside the chamber. The over all diameter of the probe was only 0.3 cm. The density and localized homogeneity of the particle cloud could be qualitatively estimated from the amount of scattered light and its intensity distribution around the illuminated spot in the cloud. A survey of the dense rotating cloud with the light probe suggested a considerable

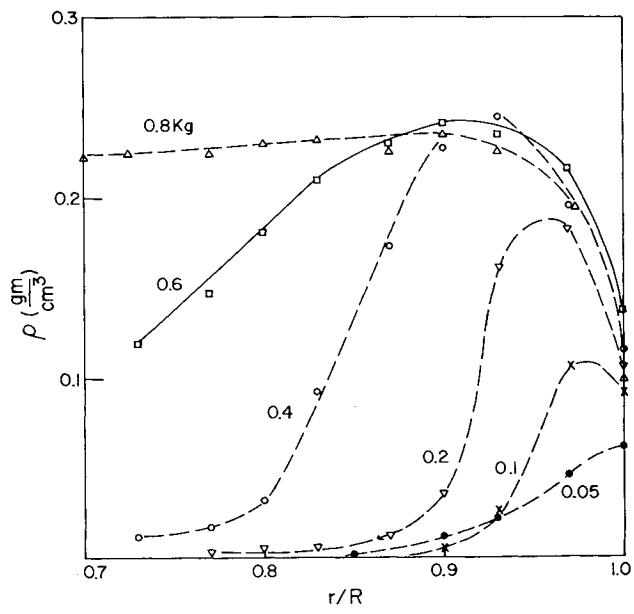

Fig. 6 Radial distributions of powder density, for various total powder masses.

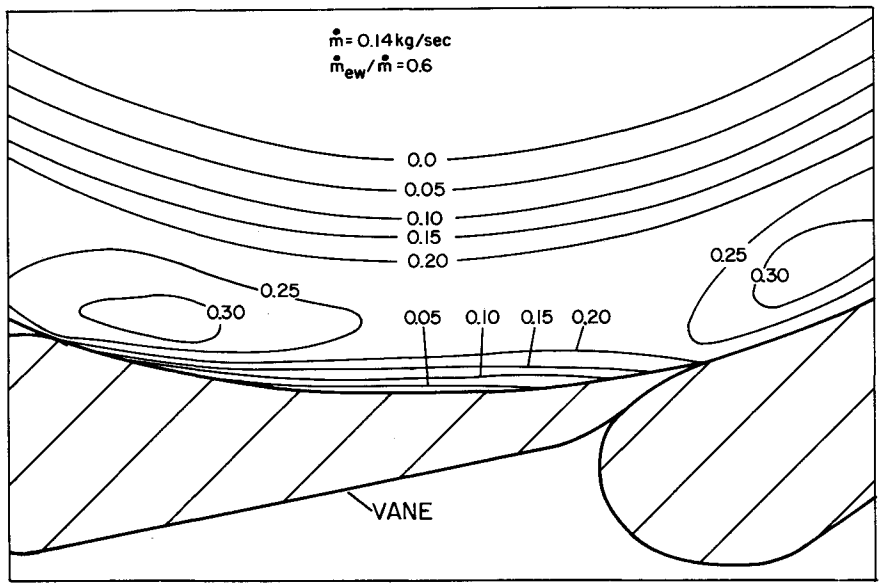

Fig. 7 Powder density contours, deduced from x-ray absorption measurements. Density values are given in gm/cm^3

degree of local uniformity in density, with little indication of bubbling or channeling of air in the dense cloud. From common vortex flow experience, it is known that Coriolis forces tend to suppress flow fluctuations and give the vortex a two-dimensional flow character,[9] i.e., with the flowfield uniform in the axial direction. This general vortex phenomenon is apparently helpful in the present case to create a rather uniform, homogeneous rotating particle cloud. In the transition region between the dense cloud and the intermediate density region, large density fluctuations were observed, apparently representing the ragged inner borderline of the cloud as seen in Fig. 3. Since the density profiles measured from x-ray absorption tests were time averaged over about 1 sec, these rapid variations would be integrated to give a smoother appearing transition, as in Fig. 6.

Angular velocity of the rotating flow was determined by inserting paddle wheels of various diameters into the vortex. The paddle wheel consisted of two oppositely positioned 1 cm square paddles connected to a teflon bearing with 0.05 cm diam wire, with a 0.3 cm diam bearing shaft located at the center of the vortex. Angular velocity of the paddle wheel was measured with either a stroboscope or a magnetic pick-up and electronic counter. Perturbation on the vortex flow generated by the presence of the paddle wheel is expected to be small in comparison to the substantial velocity fluctuations observed within the transition region. Calibration runs indicated that bearing drag had no significant effect on the speed measurements, so that paddle wheel velocity measurements should be fairly representative of actual flow velocity within the vortex. Figure 9 is a plot of paddle wheel angular velocity vs powder mass in the chamber, for a number of paddle wheel diameters. It was mentioned earlier that the first few grams of powder added to the vortex seemed to spread over the entire flow, with the exception of the vortex core. The ensuing increase in average fluid density of the vortex increases wall friction, and, along with a larger inner vortex friction due to the dispersed powder, leads to the sharp decrease in angular velocity at small powder loads observed in Fig. 9. The second downward trend in Fig. 9 is caused by the larger friction losses arising from the dense peripheral cloud (average density some 100 times that of the clean gas). Thus, the rotational speed of the dense cloud lags considerably behind that of the inner vortex region. In the transition region between the dense peripheral cloud and the inner vortex, strong turbulence (as observed in Fig. 3) transfers considerable momentum from the inner vortex region to the slow moving

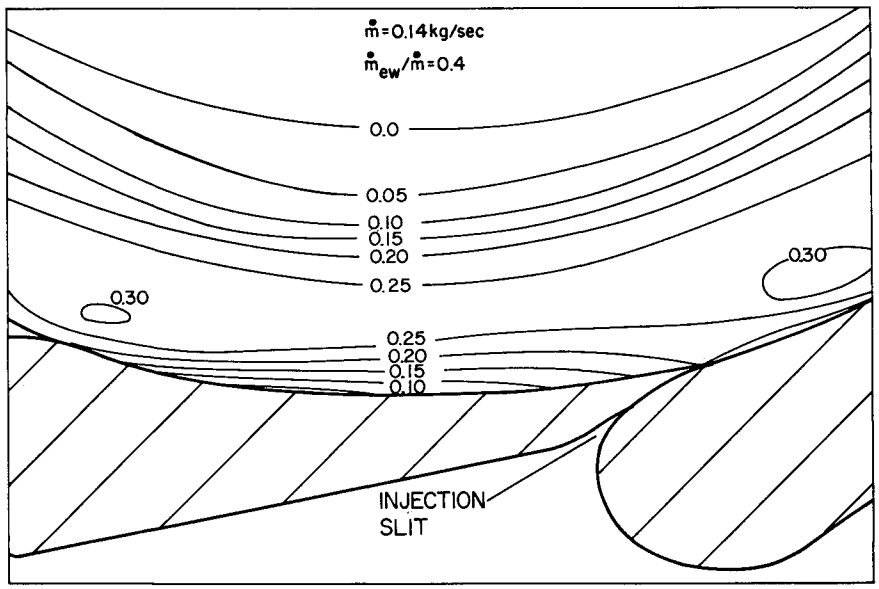

Fig. 8 Powder density contours.

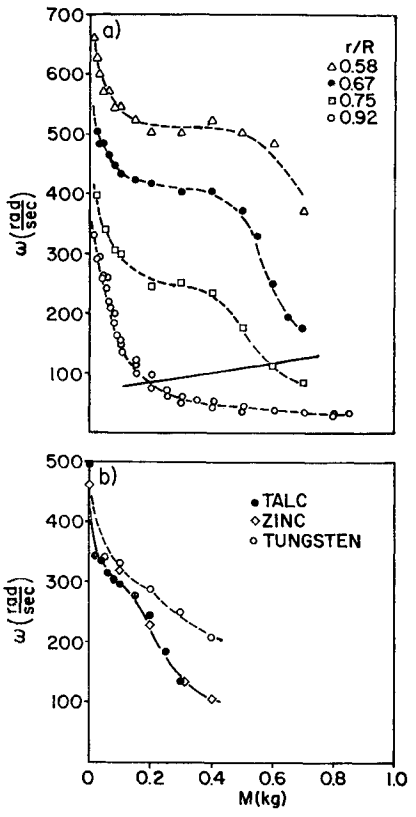

Fig. 9 Paddle wheel velocity as a function of total powder mass a) talc powder, for various radii, b) effect of different powder species, at a radius of 0.83R. Solid curve in a indicates average location of inner surface of powder bed.

peripheral cloud. Through this mechanism, some of the input momentum from end wall injection is used in driving the peripheral cloud.[7]

Analysis of Bed Fluidization

In order to extrapolate from these experimental flow conditions to probable operating conditions for a colloid core reactor, some analytical model of the multicomponent vortex must be assumed. As a first approximation to an analytical treatment of the vortex, experimental results suggest a rotating fluidized bed model. The governing equation for a plane fluidized bed is adapted to the rotating bed case[10] by replacing gravitational acceleration with centrifugal acceleration $\omega^2 r$. The resultant equation, derived in the Appendix, is

$$r^2\omega^2 = (90\mu\dot{m}/\pi h\rho_g \rho_p D^2)(1-\varepsilon)/\varepsilon^3 \qquad (2)$$

If void fraction is expressed in terms of particle density and total powder mass, Eq. 2, to first order in $(1-\varepsilon)$, indicates a similarity parameter $\rho_p D$ to relate particle characteristics to vortex flow behavior. Figure 9b shows the effect of particle characteristics on angular velocity in the vortex: the product $\rho_p D$ for talc, zinc, and tungsten is respectively 5.0, 7.0, and 25.0 mgm/cm^2 (based on mean diameter values). Therefore, one would expect the velocity data for talc and zinc to be similar, as the data indicate. The zinc data follow that of talc quite closely, both in the inner vortex region ($M < 200$ gm) and the transition region into the dense fluidized bed ($M > 200$ gm). Because of the much larger particle density of tungsten, the transition region is not encountered until $M > 400$ gm, so that the paddle wheel remains in the faster inner vortex region over the range of this experiment with tungsten.

For given chamber geometry, total powder load, particle characteristic, gas properties, and flow rate, three parameters describing the rotating fluidized bed remain undetermined: the bed void fraction ε; the inner bed radius r; and ω, the angular velocity at r. The fluidization requirement Eq. 2 must be supplemented by two additional equations to give a complete analytical description of the rotating bed. Assuming an average value for void fraction in the bed, ε is related to r and M by

$$\pi(R^2 - r^2)h\rho_p(1-\varepsilon) = M \qquad (3)$$

The third equation can be derived from consideration of momentum balance within the vortex, as explained in the appendix. By balancing momentum loss with frictional drag on the chamber walls, the following relationship is established:

$$r^2\omega = \Gamma_0(1 - \alpha M/\dot{m})/[1 + (1 - \alpha M/\dot{m})\beta M/\dot{m}] \qquad (4)$$

The constants α and β are related to the coefficient of friction, powder density, and vortex chamber dimensions, and Γ_0 is injected gas circulation. This set of simultaneous equations can be solved for r, ω, and ε. Figure 10 compares analytical results with experimental data for these three variables: gas flow conditions were $\dot{m} = 0.14$ kg/sec, $\dot{m}_{ew}/\dot{m} = 0.6$. A well-defined fluidized bed did not form until the powder load was around 100 gm, so that this analysis is not expected to be too accurate for powder mass below 100 gm. The erroneous void fraction values at low M are also at least partially due to simplifications in the frictional loss model at the periphery, as well as the sensitivity to error in r for small powder mass. Considering the complexity of the actual experiment, and the simplifying assumptions made to arrive at the calculated results,

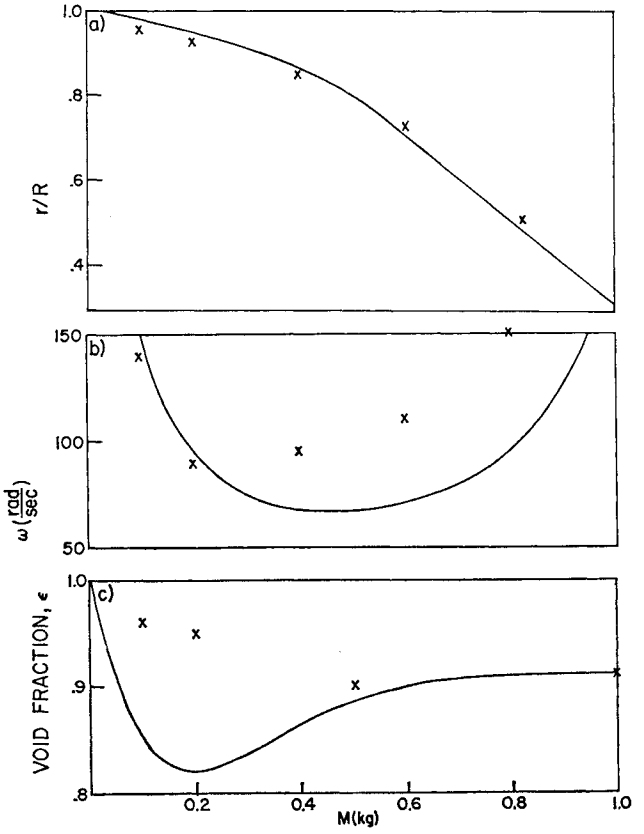

Fig. 10 Comparison of calculated and experimental values for rotating fluidized bed parameters a) inner bed radius, b) angular velocity at inner bed surface, c) average void fraction of bed.

the analytical predictions are in reasonably good agreement with experiment. The success exhibited here in predicting these rotating bed parameters encourages application of this line of analysis to a study of flow requirements for the colloid core reactor concept.

Implications for the Colloid Core Reactor

As an example of possible extrapolation from our present experiment to operating conditions of the colloid core reactor, a hypothetical engine will be assessed, with thrust of 20,000 lb force, and specific impulse of 1000 lb_f-sec/lb_m. A mass flow rate of 10 kg/sec would then be required. Taking hydrogen as operating medium and assuming a temperature of 3300°K, the dynamic viscosity of the gas flow in the reactor would be about 0.04 centipoise, and gas density at a median cavity pressure of 100 atmospheres would be about 1 kg/m^3. A uranium carbide alloy, (1U − 10Zr) C, has been proposed[11] as a possible fuel for the colloid core reactor because of its low uranium equilibrium vapor pressure. Material density of this fuel would be about 8 gm/cm^3, near the density of zinc. For convenience in relating the behavior of the particulate fuel to our observations of zinc particles, the fuel particle diameter will be taken as 10μ. For this example, the reactor radius is taken as 30 cm, with an axial length of 30 cm, and an inlet velocity of 100 m/sec is given for tangential gas injection.

Critical mass calculations for a cavity radius of 30 cm and axial length of 12 cm indicate a uranium mass requirement of about 3 kg.[11] Critical mass requirement for the longer chamber used in the present example is probably lower than the 3 kg figure, but for a conservative estimate, 3 kg uranium mass, for a total fuel load of 30 kg, will be assumed. Applying the parameters to Eq. (2–4), inner bed radius, angular velocity, and void fraction can be calculated. The various extrapolated flow parameters for the reactor are compared with experimental conditions in Table 1. Note that the particle volume fraction $(1 - \varepsilon)$ required by this fuel load is well below the 10% value attained in our present experiments.

The power output required by the engine performance specification is about 600 mw, with a reactor power density of about 10^4 mw/m^3. The average temperature differential between particles and gas is derived in the Appendix, indicating a temperature difference on the order of 20°K between fuel particles and propellant gas for this reactor. The total pressure drop needed to fluidize the particle bed under the prescribed conditions is about 33 atm.

If the zinc particle loss rate given in Fig. 5 is linearly scaled to the larger gas flow rate per unit area under consideration for the reactor, a fuel loss of about 30 gm/sec is predicted, for a uranium loss rate of 3 gm/sec. Vaporization loss for uranium has been estimated[12] at roughly 100 gm/sec at an operating temperature of 3300°K, so that particulate loss will be small in comparison to vaporization.

Table 1 Flow parameters

	Experimental vortex	Projected reactor
R	0.15 m	0.30 m
h	0.06 m	0.30 m
$\dot{m}/A$	1.7 kg/m^2 sec	17.7 kg/m^2 sec
ρ_g	1.2 kg/m^3	1.1 kg/m^3
μ	0.02 centipoise	0.04 centipoise
ρ_p	7.0 gm/cm^3	8 gm/cm^3
D	10 μ	10 μ
M	0.8 kg	30 kg
ε	0.9	0.95
r	0.08 m	0.13 m
ω	150 rad/sec	450 rad/sec

Conclusion

Our experiments with two component vortex flows, when extrapolated to the operating range of a colloid core reactor, project a reasonable degree of optimism concerning the ultimate feasibility of such a system. The projected reactor size is modest, no problem appears in fluidizing and rotating the required fuel load, and reactor power density is well within the heat-transfer capacity of the fluidized bed. Rough estimates of particulate fuel losses indicate that uranium loss rate will be governed primarily by materials problems, rather than aeromechanical considerations. Many problems concerning the generation and transfer of power within a rotating fluidized bed are yet to be answered, but the basic concept of maintaining a fluidized vortex flow of high-particle density to provide nuclear propulsion appears to be sound.

Appendix

Fluidization Equation

The pressure drop per unit length $\Delta P/\Delta L$ of a columnar fluidized bed is given by[13]

$$\Delta P/\Delta L = (180\mu v/D^2)(1 - \varepsilon)^2/\varepsilon^3 \tag{A1}$$

where v is the superficial gas velocity. In the rotating fluidized bed, v corresponds to the radial inflow velocity, and the pressure drop must balance centrifugal force acting on the bed. With the continuity equation for the radial gas flow, the fluidization equation is

$$r\omega^2 = (\dot{m}/2\pi rh\rho_g)(180\mu/\rho_p D^2)(1 - \varepsilon)/\varepsilon^3 \tag{A2}$$

Momentum Balance Equation

Angular momentum input to the vortex comes exclusively from gas injection, while momentum loss is due to frictional interaction of the particle-gas medium with the chamber walls. In this analysis of the momentum loss, several simplifying assumptions are made: all gas inflow is assumed to come from peripheral injection (with the gas flow rate taken as the sum of the actual peripheral and end wall injection rates[7]); wall friction is taken as proportional to flow density, with constant frictional coefficient c_f; and particle density is assumed uniform within the powder bed, with a reduced density at the periphery. Equating the change of angular momentum across a cylindrical section of width δr to the wall friction torque within that region, the following is obtained

$$\dot{m}\delta\Gamma_r = 2\pi c_f \rho \Gamma_r^2 \delta r \tag{A3}$$

By integration of this equation from the inner radius of the powder bed r to the periphery R, the circulation (ωr^2) of the powder flow at the inner radius is found

$$\Gamma_r = \Gamma_R/[1 + 2\pi\bar{\rho}c_f(R - r)\Gamma_R/\dot{m}] \tag{A4}$$

At the periphery, frictional loss along the vane surfaces causes a reduction in the inlet circulation from Γ_0 to Γ_R, so that

$$\Gamma_R = (1 - \pi c_f \rho_R h\Gamma_0/\dot{m})\Gamma_0 \tag{A5}$$

Using Eq. 3 to relate mean powder density to total mass, and assuming that ρ_R is proportional to $\bar{\rho}$

$$\omega r^2 = \Gamma_0(1 - \alpha M/\dot{m})/[1 + (1 - \alpha M/\dot{m})\beta M/\dot{m}]$$
$$\alpha \simeq c_f(\Gamma_0/R^2)\rho_R/\bar{\rho} \tag{A6}$$
$$\beta \simeq c_f\Gamma_0/Rh$$

The injected circulation Γ_0 was estimated from experiments to be 8.5×10^4 cm^2/sec. An estimate of c_f was obtained from experimental data given in Ref. 14, with a value of $c_f = 0.003$. The density ratio $\rho_R/\bar{\rho}$ was taken as 0.1. This value was chosen somewhat lower than that indicated by Fig. 6, in an

effort to reflect the low-powder density existing near the gas injection slot (see Fig. 7).

Heat Transfer in Particle Cloud

If ΔT_{Trans} is the average temperature difference between particles and gas, and ΔT_{gas} is the temperature change of the gas as it flows through the particle bed, then under equilibrium conditions

$$h_c A_{\text{tot}} \Delta T_{\text{Trans}} = \dot{m} c_p \Delta T_{\text{gas}} \tag{A7}$$

c_p is specific heat of gas, and A_{tot} is total surface area of particles. Heat transfer coefficient h_c for particles in a fluidized bed can be obtained from experimental results[15] correlated between Nusselt number Nu and Reynolds number Re for the range $Re = 0.1$ to 10, by $Nu = 0.017\ Re$. Incorporating this relationship with Eq. (A7) leads to

$$\Delta T_{\text{Trans}}/\Delta T_{\text{gas}} = [10/(1-\varepsilon)][D/(R-r)]Pr \tag{A8}$$

Pr is Prandtl number for the gas, approximately equal to 0.6 for hydrogen at reactor conditions. The Nusselt number associated with the average heat-transfer coefficient for the fluidized bed is appreciably below the minimum value of a single sphere, $Nu = 2$. This fact is explained[15] by gas bypassing in the fluidized bed, so that all particles are not equally exposed to the through-flowing gas. This condition may be useful in determining the uniformity of the rotating fluidized bed from heat-transfer measurements.

References

[1] Clement, J. D. and Williams, J. R., "Gas Core Reactor Technology," Reactor Technology, Vol. 13, No. 3, 1970, pp. 226–251.

[2] Hatch, L. P., Regan, W. H., and Powell, H. R., "Fluidized Solids as a Nuclear Fuel for Rocket Propulsion," *American Rocket Society Journal*, Vol. 31, No. 4, April 1961, pp. 547–548.

[3] Jackomis, W. N. and von Ohain, H. J. P., "Aeromechanical Characteristics of Nuclear Reactor Cavities Using Colloidal Fuels," AIAA Paper 70-1222, Houston, Texas, 1970.

[4] Rosenzweig, M. L., Lewellen, W. S., and Ross, D. H., "Confined Vortex Flows with Boundary-Layer Interaction," *AIAA Journal*, Vol. 2, No. 12, Dec. 1964, pp. 2127–2134.

[5] Poplawski, R. and Pinchak, A. C., "Aerodynamic Performance of Reversed Flow Vortex Chambers," TR ARL 65–219, 1965, Aerospace Research Labs., Wright-Patterson Air Force Base, Ohio.

[6] Shelnutt, J. W., "Particle Size Analysis by Sedimentation," TR ARL 71-0134, 1971, Aerospace Research Labs., Wright-Patterson Air Force Base, Ohio.

[7] Turman, B. N. and Hasinger, S. H., "Experimental Flow Studies of the Colloid Core Reactor Concept," *2nd Symposium on Uranium Plasmas: Research and Applications*, American Institute of Aeronautics and Astronautics, Nov. 1971, pp. 269–275.

[8] Rowe, P. N. and Partridge, B. A., "An X-Ray Study of Bubbles in Fluidized Beds," Transactions of the Institution of Chemical Engineers, Vol. 43, 1965, pp. 157–175.

[9] Taylor, G. I., "Experiments on the Motion of Solid Bodies in Rotating Fluids," *Proceedings of the Royal Society*, Vol. A104, 1923, pp. 213–218.

[10] Lindauer, G. C., Tichler, P., and Hatch, L. P., "Experimental Studies on High-Gravity Rotating Fluidized Beds," Rept. BNL 50013 (T-435), 1966, Brookhaven National Labs., N. Y.

[11] Tang, Y. S., Stefanko, J. S., Dickson, P. W., and Drawbaugh, D. W., "An Engineering Study of the Colloid-Fueled Reactor Concept," *Journal of Spacecraft and Rockets*, Vol. 8, No. 2, Feb. 1971, pp. 129–133.

[12] Westinghouse Astronuclear Laboratory, "Engineering Study of Colloid Fueled Nuclear Rocket," TR ARL 69-0234, Dec. 1969, Aerospace Research Labs., Wright-Patterson Air Force Base, Ohio.

[13] Zenz, F. A. and Othmer, D. F., *Fluidization and Fluid-Particle Systems*, Reinhold, N. Y. 1960, p. 177.

[14] Wen C. and Simons, H. P., "Flow Characteristics in Horizontal Fluidized Solids Transport," *AIChE Journal* Vol. 5, No. 2, June 1959, pp. 263–267.

[15] Zenz, F. A. and Othmer, D. F., *Fluidization and Fluid-Particle Systems*, Reinhold, N. Y., 1960, pp. 433–436.